Energy Engineering

Tech Science Press

https://doi.org/10.32604/ee.2026.076901

ARTICLE

Research on Numerical Calibration of Power in Complex Terrain Wind Farms Based on Model Reconstruction

Xin Guan*, Dechen Kong, Bo Liu, Hao Tang and Longlong Zong

Institute of New Energy, Shenyang Institute of Engineering, Shenyang, China

*Corresponding Author: Xin Guan. Email: xin_guan@sina.com

Received: 28 November 2025; Accepted: 23 March 2026; Published: 12 November 2026

ABSTRACT: Unlike flat terrain, when air flows through mountainous terrain, it is affected by undulating terrain and ground obstacles, forming complex wind field basins. This leads to the actual power generated by wind turbines being lower than the predicted power. Due to the complexity and uncertainty of the terrain and environment of wind farms, there is a significant difference between the measured power of wind farms and the actual output power of wind turbines. Therefore, studying the influence of complex terrain on wind speed in wind farms is of great significance for the site selection and construction of wind turbines. This paper adopts numerical reconstruction of the actual complex mountain terrain to determine the computational domain of the complex terrain, and compares the existing data to verify the reliability of the model. By changing the ground roughness of the mountain model, the influence of roughness on the wind speed variation at different measurement points in the mountain was analyzed. The variation characteristics of wind speed at various environmental measurement points under different terrain positions and wind turbine operation conditions under complex terrain conditions were mainly studied. Through the numerical calculation of wind speed measurement data and the wind speed variation data table of wind speed measurement points, the accuracy of wind power numerical calibration in wind farms under complex terrain conditions was studied.

KEYWORDS: Numerical simulation; reconstruct complex terrain; wind turbine; aerodynamic characteristics; power calibration

1 Introduction

With the rapid development of the wind power industry, researchers and builders have begun to pay attention to some complex terrain areas in order to better estimate the distribution of wind resources and their impact on wind flow. When the airflow approaches a flat ground, it flows along the ground. As the ground slope increases, the airflow will separate or deviate from the surface, often generating vortices. At the same time, the intensity of turbulence will increase. At this point, the wind speed will not follow the typical linear law, thus making the problem very complicated when establishing the flow field model of a wind farm and assessing wind resources [1]. Field measurement is carried out by establishing measurement points on a certain complex terrain and monitoring the wind speed changes in the terrain area to obtain the wind field model under complex terrain. Although this method can accurately obtain the wind field model under complex terrain, it often takes a long time, consumes human and material resources, requires processing and verification of a large amount of data, and is restricted by the experimental site. Numerical simulation is to use the Computational Fluid Dynamics (CFD) method to conduct numerical modeling of the study area, simulate the aerodynamic characteristics of the wind field when the airflow passes through complex

Copyright © 2027 The Authors. Published by Tech Science Press. This work is licensed under a Creative Commons Attribution 4.0 International License, which permits unrestricted use, distribution, and reproduction in any medium, provided the original work is properly cited.

mountainous areas on the computer, and obtain the wind field model when the airflow passes through complex regions. This method needs to be verified through wind tunnel tests or on-site measurements, and parameters should be adjusted to obtain accurate aerodynamic characteristics of typical mountain wind farms. Compared with the above three methods, numerical simulation has the advantages of high accuracy, short cycle and high efficiency [2].

Wind farm wind tunnel testing is an experimental method in which a wind turbine model is placed in a wind tunnel to study gas flow and its interaction with the model, and to understand the aerodynamic characteristics of the actual wind turbine. Wind tunnel tests can precisely control parameters, enabling researchers to systematically study the aerodynamic characteristics of wind turbines under the influence of terrain. This method was introduced into the wind power field in the 1950s. For the wind tunnel test research under complex terrain, Duque et al. [3] conducted a comprehensive analysis of the National Renewable Energy Laboratory Phase VI (NREL Phase VI) wind turbine through wind tunnel tests, obtained a large amount of data, and provided important data for the later research. Kondo et al. [4] conducted wind tunnel tests on two-dimensional slopes of different slopes to study the terrain acceleration effect of two-dimensional slopes at different slopes. Cao and Tamura [5] studied the influence of surface roughness on the upwind acceleration effect of two-dimensional steep slopes through wind tunnel experiments, and discussed the acceleration ratio and turbulent structure. The results showed that the presence of the mountain body would significantly accelerate the air flow, and the turbulence intensity would also increase accordingly. Cao's research results also successfully verified Ishihara T's achievements [6]. Tian et al. [7] conducted wind tunnel experiments to study the wake characteristics and power performance of five wind turbine arrays located on the two-dimensional Goss Hills. They found that the wind speed on the summit and the windward side was relatively high while the turbulence intensity was relatively low, which was suitable for the deployment of wind turbines. Hyvärinen and Segalini [8] measured the thrust and power coefficient of two wind turbines located on a hilly terrain composed of multiple sinusoidal hills through wind tunnel tests. They pointed out that due to the existence of continuous hills, the wake recovery of the upstream wind turbines became more rapid, which had a favorable impact on the power performance of the downstream wind turbines.

Numerical computing is a method that relies on computer algorithms and numerical analysis to solve mathematical equations and physical problems. It is based on the discretization of mathematical models, transforming continuous mathematical problems into discrete numerical problems. Studying the flow field through numerical calculation methods not only enables better control of variables and effective reduction of uncertainties during the numerical calibration process, but also allows for calculation and analysis in extreme cases, making the experimental data more comprehensive. Shapiro et al. [9] proposed a vortex cylinder model to quantify the vorticity shed when the filter force distribution is applied on the actuator disc in order to correct the simulation error caused by the actuator disc model. Then, the correction coefficients of the numerical simulation are derived by using this model. Karim et al. [10] used the Reynolds-Averaged Navier-Stokes (RANS) model to simulate the area near two consecutive hills. These analyses provided simple estimates of turbulent kinetic energy k for the calculation of wind loads on the tower, thereby studying the restoration effects of mountain vegetation with different slopes and different slope height ratios. Tian et al. [11] conducted an experimental study on the aerodynamics and wake interference of wind turbines on two-dimensional hills with different slopes. This not only provides a database for verifying wake models and numerical simulations, but also can be used to optimize the layout of wind turbines located on complex terrains to achieve higher power output and better durability. Yan et al. [12] conducted systematic atmospheric boundary layer (ABL) wind tunnel experiments to investigate the aerodynamic and wake characteristics of wind turbines, analyzing the combined influence of atmospheric turbulence and hilly terrains on the flow field and power performance. Chen and Ishihara [13] conducted a detailed analysis

of the influence of factors such as grid resolution, turbulence models, and terrain slope variations on the accuracy of numerical simulation wind fields. They adopted the local smoothing method at the separation point at the top of the slope to analyze the characteristics of the wind field at the top of the slope Yamaguchi et al. [14] reconstructed actual complex terrain and developed a microscale flow model to study the wind speed distribution and wake structure evolution of wind farms under the combined effects of topography, dynamic atmospheric stability, and turbine wakes. Li et al. [15] restored real complex terrain based on elevation data and studied the wind speed distribution and wake structure evolution law of wind farms under actual complex terrain and dynamic wind speed.

This paper proposes a method for reconstructing complex terrain and verifies the rationality of the model. After simplifying the model, a specific analysis is conducted on a certain working condition. Through a large number of numerical modeling and simulation calculation methods, the wind turbine and the complex terrain are jointly calculated. The main research focuses on the influence of the wind turbine and the complex terrain on wind speed under various working conditions.

2 Numerical Reconstruction of Complex Terrain

The terrain in mountainous areas is usually high, and there are parts with relatively better wind resources. However, at the same time, the terrain in mountainous areas is complex, the flow field distribution is uneven, and the randomness of air flow disturbances is strong, making wind conditions difficult to predict. Moreover, the site selection of wind farm units in mountainous areas is often restricted, which leads to the frequent occurrence of wake effects among units, resulting in a decline in the power generation performance of the units and affecting the economic benefits of wind farm operation. Therefore, studying the characteristics of wind farms in complex terrains has practical and feasible significance [16]. This chapter adopts CATIA as the terrain modeling method for wind farms, proposes two terrain reconstruction methods and verifies them, and takes the most cost-effective method to analyze the subsequent working conditions.

2.1 Determination of Terrain Complexity

Terrain complexity is the result of the fusion expression of multiple terrain factors. To avoid compressing or losing information about the complexity of the terrain, this paper adopts a weighted approach to combine various terrain factors. Based on principal component analysis, the objective weights of each core factor are obtained, and the terrain complexity model formula is constructed [17]:

$$TCI = 0.0033TCD - 0.0038SOA + 0.0541SL + 0.034SLO + 0.0027TPI + 2.089PLC \quad (1)$$

TCI is the comprehensive coefficient of the mean standardized core terrain factor index. When $TCI < 0.1$, there is no obvious undulation in the terrain, presenting the terrain characteristics of plains or basins, and the complexity of plains is lower than that of basins. When $0.1 \leq TCI < 1.8$, the terrain has a certain degree of undulation and folds. When $TCI \geq 1.8$, the undulation of the terrain and the scale of the mountain body are relatively large, and the degree of folding is more obvious, presenting the characteristics of mountainous terrain. In this paper, the area with $TCI \geq 1.8$ accounts for 83.7% of the entire area, meeting the complex mountainous terrain characteristics.

2.2 Terrain Reconstruction Methods

To simulate the flow field of a wind farm under the influence of complex terrain, three-dimensional modeling of the actual terrain is required. The complex terrain three-dimensional model is generated through point cloud modeling and parametric modeling methods to conduct numerical calculations on the

terrain wind farm. This article selects a mountainous area in Zhejiang Province for analysis. The regional range is 1.1 km × 1.1 km × 0.6 km. The actual landform is shown in Fig. 1.



Figure 1: Physical topographic map of wind farm.

Parametric reconstruction method

Parametric reconstruction method is a design process based on mathematical functions, which writes the project itself as a function and process. By modifying the initial conditions and obtaining the project results through computer calculation, it realizes the automation of the wind farm modeling process. The core of parametric modeling for wind farms is variable Design, that is, variables control parameters, and each variable controls or correlates certain properties in the terrain factors of the wind farm. The Generic Shape Design (GSD) method is applied to achieve the mixed modeling requirements of the terrain environment of the wind farm. By adjusting control parameters such as Angle, direction and length, the needs of terrain modules for wind power calibration in different wind farms can be met. The parametric terrain modeling method is highly flexible and operable. It can not only quickly generate terrain models using known data, but also simplify operation steps for convenient modification. The specific operation process and the parametric reconstruction of the entity model are shown in Fig. 2.

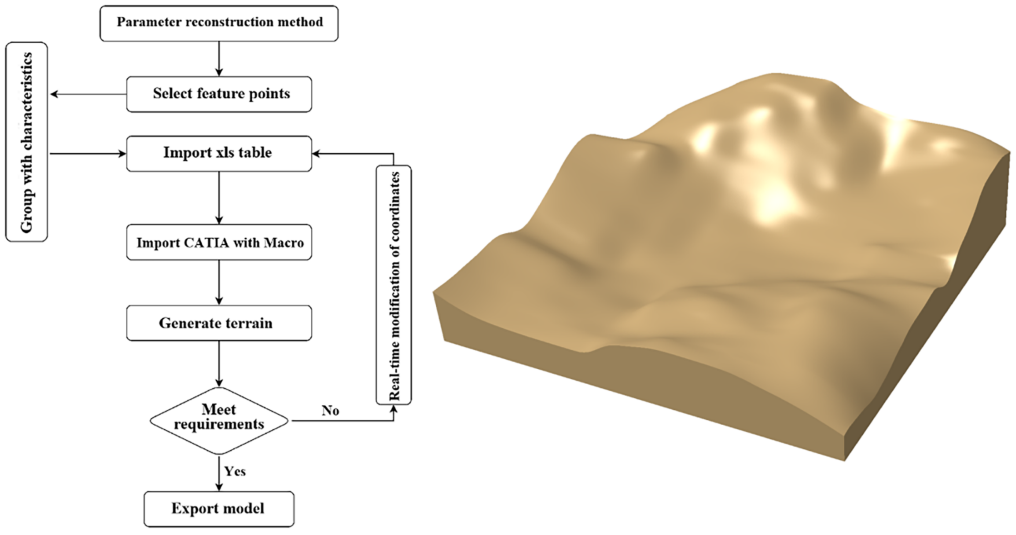


Figure 2: Workflow and terrain digital model of parametric reconstruction method.

At the same time, due to the adjustment of the constructed terrain coordinate value data, the workload of reconstructing the terrain surface is large and the flexibility is poor. Therefore, parametric modeling can conveniently solve the above problems and thereby achieve the maximization of engineering benefits.

3 Calculation Method and Verification

3.1 Wind Shear Model

Ground obstacles (such as grasslands, crops, forests, and buildings) can generate friction on air flow, impede the movement of wind, and reduce the wind speed near the ground. The rate of wind speed decrease with the increase of ground height until the height reaches a certain value, at which point the influence of surface roughness on wind speed can be ignored. The layer of the atmosphere affected by surface frictional resistance is called the atmospheric boundary layer [18]. Within the atmospheric boundary layer, the average wind speed varies with height. This variation pattern is known as the wind shear effect or wind speed profile. In the atmospheric boundary layer, the variation of wind speed is described by wind shear or wind speed profile, which is expressed by logarithmic law or exponential law, thereby expressing the variation law of wind speed with height in the atmospheric environment. For the neutral atmosphere, the wind speed profile within the atmospheric boundary layer can be represented by a logarithmic function. For the $k-\varepsilon$ turbulence model, Richards & Hoxey proposed the logarithmic function of wind shear velocity, the formula for turbulent kinetic energy, and the $k-\varepsilon$ turbulence dissipation rate formula

$$\overline{u}(z) = \frac{u_*}{K} \ln\left(\frac{z+z_0}{z_0}\right) \tag{2}$$

In the formula, z represents the height above the ground surface. z_0 is the surface roughness length, taken as 0.1 m. u_* is the surface friction velocity taken as 0.47 m/s; K is the von Karman constant. If the value at the center of the wind turbine is 8 m/s, the von Karman constant is taken as 0.4.

In this paper, the turbulent kinetic energy k is defined as follows, and C_μ is the turbulence model constant with the default value of 0.09.

$$k = \frac{u_*^2}{\sqrt{C_\mu}} \tag{3}$$

The turbulent kinetic energy dissipation rate is:

Generally speaking, the top of the atmospheric boundary layer is where the turbulent kinetic energy is the lowest or even disappears. However, when the observed height exceeds this range, the velocity will not change, and the turbulent kinetic energy and dissipation rate will become extremely small or even disappear. It can be calculated that the velocity profile at the entrance is shown in Fig. 3.

3.2 Grid Division and Independence Verification

The accuracy of numerical simulation mainly depends on the adoption of turbulence models, simulation methods, and the precision of the grid. Among them, high-quality grids are the key to ensuring the accurate simulation of the aerodynamic performance of wind turbines. Currently, the main types of grids include structured grids and unstructured grids.

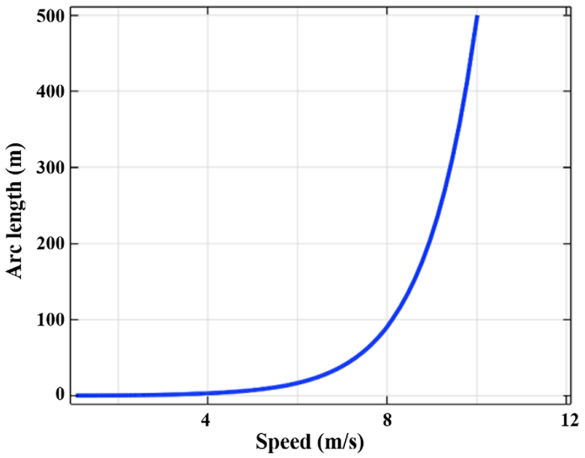
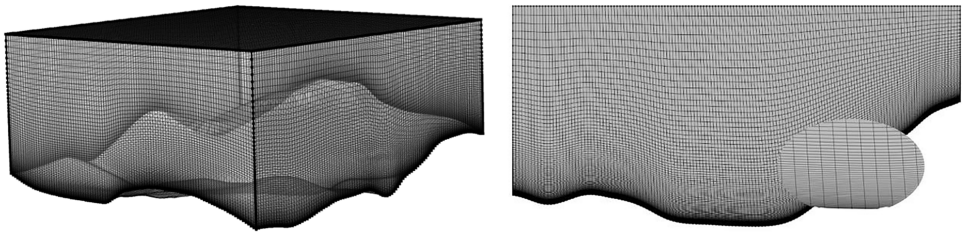


Figure 3: Wind speed contour line at air inlet.

Unstructured grids are suitable for complex geometries and irregular computing domains, offering greater flexibility and adaptability. In some cases, unstructured grids may lead to unstable values or increased numerical errors; Structured grids have a regular layout, which helps to achieve simple boundary conditions and mathematical expressions. When dealing with complex geometries, structured meshes may cause the meshes to become unreasonably dense or sparse, making it difficult to adapt to irregular or non-regular computational domains. Due to the relatively uniform terrain structure, a structured hexahedral mesh can be adopted for analysis. Fig. 4 shows the mesh in the fluid domain.



(a) The whole **(b)** Analytical cross-section

Figure 4: Fluid domain grid.

The hexahedral structured grid division of the computing domain is completed through the method of mapping and sweeping, and multiple groups of grids with different grid densities are set up to conduct the grid independence test. This paper selected seven different density grids of 2.56, 2.95, 3.19, 3.41, 3.5, 3.83 and 4.05 million. As the number of grids increased, when the number of grids reached 3.83 million, the wind speed change tended to be horizontal, meeting the grid independence verification. Finally, the number of grids of 3.83 million was determined, as shown in Fig. 5.

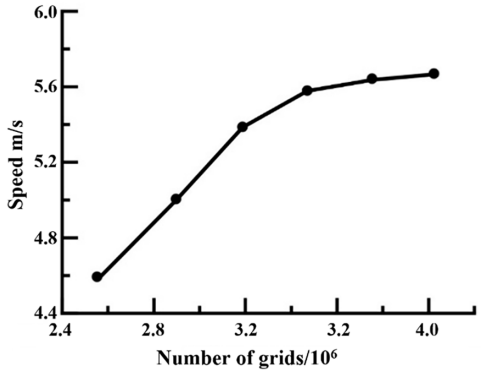


Figure 5: Grid verification.

4 Analysis of Factors Influencing Air Flow Velocity

In the atmospheric boundary layer, the distribution of velocity in the normal z direction of the wall surface satisfies Formula (3). When the surface roughness z_0 changes, the velocity in the boundary layer will also change accordingly. Therefore, it is necessary to conduct in-depth research on the laminar flow field at the atmospheric boundary under different surface roughness conditions [19].

4.1 Calculation of Flow Velocity with Different Roughness

When wind passes through narrow passages between mountains, its wind speed will increase. This phenomenon is known as the wind acceleration effect. The effect of the summit is the same as that of the narrow passage, that is, the wind speed at the summit also has an accelerating effect, as shown in Fig. 6.

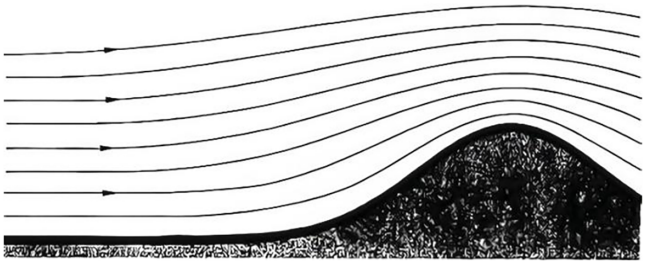
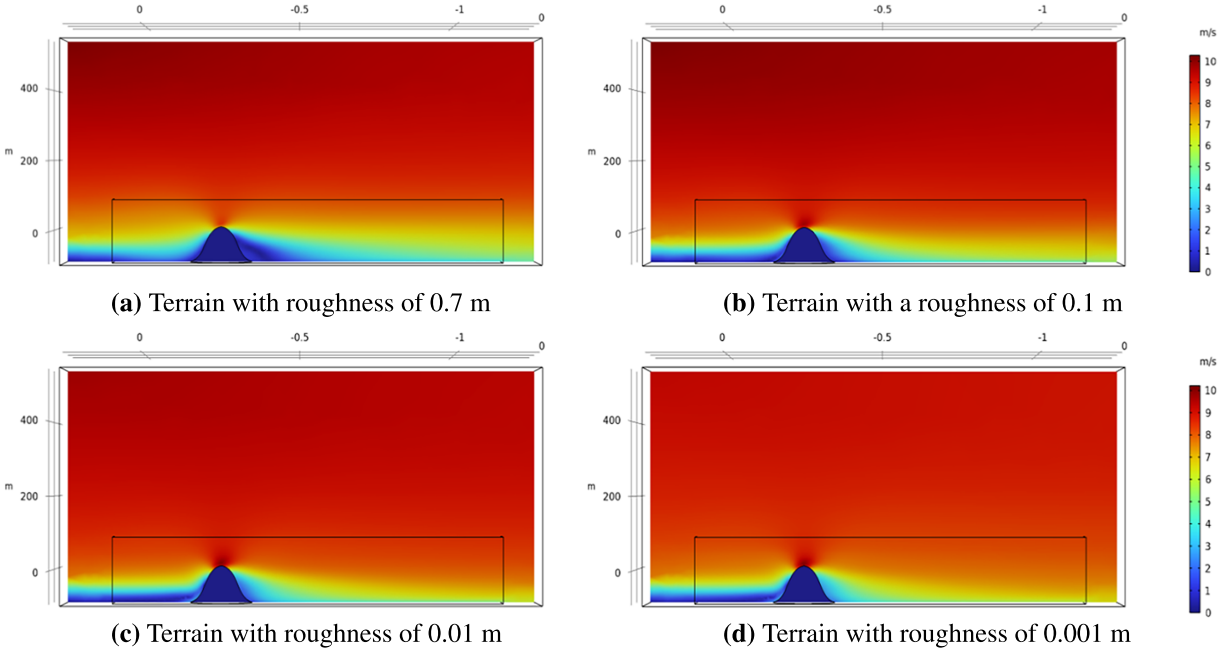


Figure 6: Schematic diagram of wind acceleration streamline.

Fig. 7 shows the velocity cloud map of the terrain section under different roughness. It can be seen from the figure that the wind accelerates along with the terrain on the windward slope of the mountain and reaches the peak velocity near the summit. On the leeward slope, due to the shielding effect of the mountain on the wind, a recirculation zone is formed behind the mountain. In this area, the flow lines are spirally distributed, and the wind speed drops sharply and slowly recovers downstream of the mountain. It can be seen that the existence of the reflux zone has significantly raised the streamline trajectory behind the mountain.

Fig. 7a–d respectively correspond to the velocity cloud diagrams of the central symmetry plane under the incoming flow conditions subjected to wind shear, with roughness z_0 being 0.7, 0.1, 0.01, and 0.001 m. It can be seen from the figures that the mountain has the greatest influence on the velocity distribution on the leeward side, followed by the velocity at the mountain top. On the windward side, the acceleration effect is obvious near the ground on the mountain top. A velocity reflux zone is formed on the leeward side

due to the compression effect of the mountain, which gradually increases the wind speed and reaches its maximum value at the summit. As the flow continues to develop, a large-scale velocity reflux area is generated on the leeward side of the mountain. The incoming wind speed cannot be directly transmitted down along the mountain surface. It can only flow downward from the top of the slope at the height where the flow is faster, resulting in a vertical upward velocity direction at the foot of the mountain on the leeward side. Under the action of shear force, both the amplitude of wind speed pulsation and the amplitude of longitudinal energy transfer decrease. When the incoming flow flows above the return zone, it will not mix with the low-wind-speed area.



(a) Terrain with roughness of 0.7 m

(b) Terrain with a roughness of 0.1 m

(c) Terrain with roughness of 0.01 m

(d) Terrain with roughness of 0.001 m

Figure 7: Velocity cloud map of terrain sections under different roughness.

It can be seen from Fig. 7a,b that the velocity reflux zone on the leeward side of the terrain with a roughness of 0.1 m is reduced compared to z_0 = 0.7 m, and the wind speed acceleration effect near the ground on the mountain top is increased. The reason for this is that the blocking effect caused by the roughness is weakened. After the incoming wind passes through the mountain top and reaches its maximum wind speed, due to the lack of pulsating energy exchange, under the blocking and friction of the mountain itself, the near-ground speed at the foot of the leeward side of the mountain is zero. The wind speed at the summit of the main wind direction exchanges with the leeward side and the near-ground speed, which in turn causes the speed to flow back. The roughness of the terrain causes the wind speeds at different heights near the ground to rub against each other, further reducing the wind speed. Therefore, the greater the roughness, the slower the recovery of the backflow effect.

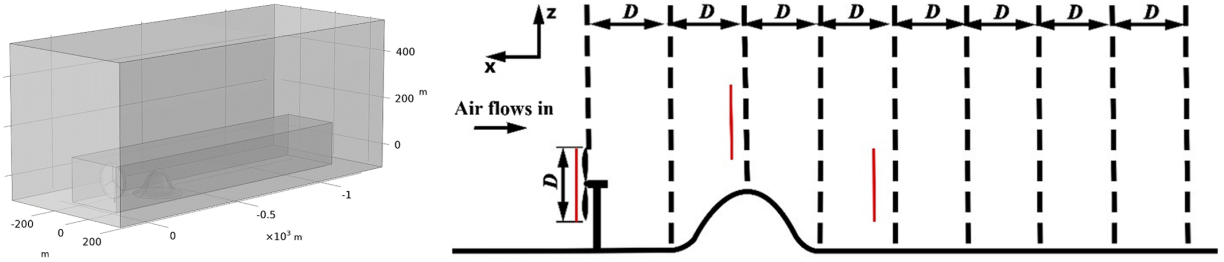
Fig. 7c,d respectively correspond to the velocity distribution of wind shear incoming flow under the terrain roughness with roughness z_0 of 0.01 and 0.001 m. Due to the reduction of terrain roughness, the wind acceleration effect near the ground at the mountain top is further enhanced, and the backflow area in the leeward zone is further reduced. Its influence is significantly lower than that of roughness z_0 = 0.7 and 0.1 m.

4.2 Calculation of Flow Velocity in the Operating State of Wind Turbines

Combine the wind turbine model with the mountain model, place the wind wheel in the rotation domain, and use the frozen rotor technology to calculate the wind speed changes of the wind turbine in different operating states, as well as in the upstream, summit and downstream areas of the mountain. When calculating, grid densification is carried out for the rotation domain and the tail basin. The ground roughness z_0 is selected as 0.1 m, the inlet wind speed is set as the wind shear function, and the wind speed at 90 m above the ground is 8 m/s.

(1) The wind turbine is located upstream of the terrain

As shown in Fig. 8, it is a schematic diagram of the computational fluid domain and analysis cross-section of the wind turbine located upstream of the mountain. The center of the wind turbine is set as the coordinate origin, and the wind speed measurement area is the diameter D of the wind turbine (the part in the red area).



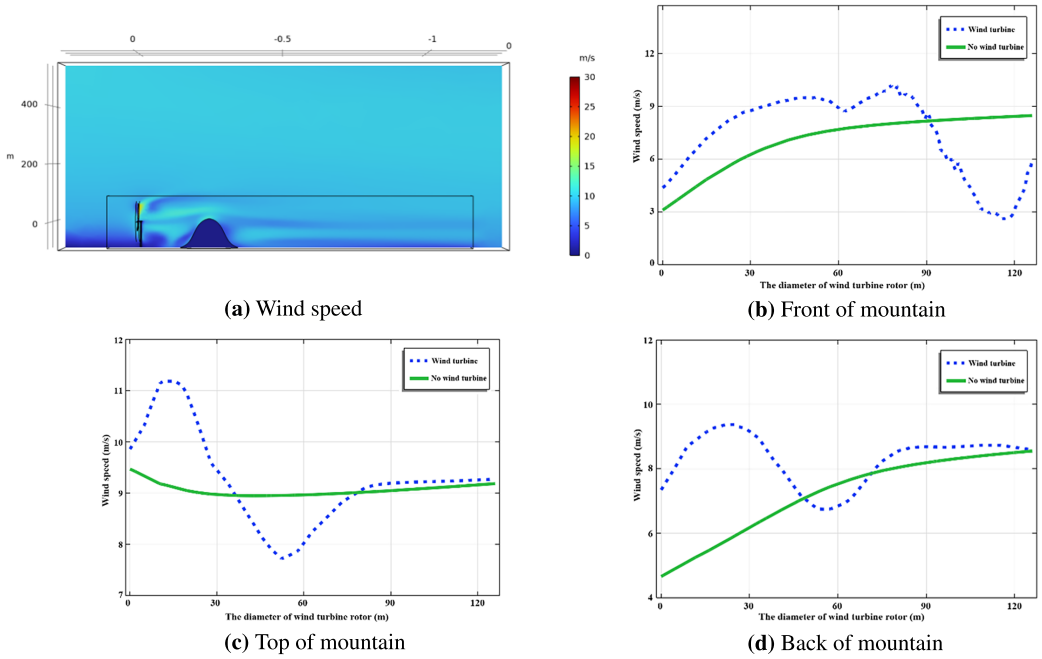
(a) Fluid calculation domain **(b)** Analytical cross-section

Figure 8: Fluid calculation domain and analysis cross-section.

Fig. 9a shows the velocity cloud diagram of the central symmetry plane of a wind turbine in a rotating state. The wake trajectory of the wind turbine can be clearly seen in the figure. Due to the rotation of the wind turbine and the effects of wind shear and wind acceleration, the wake of the wind turbine gradually becomes disordered, and the boundary becomes blurred. The overall trend is a significant rise under the action of the windward slope and a gradual decline after passing through the summit. Fig. 9b–d respectively show the wind speed curves of the wind turbines in operation at the three positions in front of the mountain, at the top of the mountain, and behind the mountain. The wind speed at the position in front of the mountain is the wind speed in front of the diameter of the wind turbine blade. Due to the rotation of the wind turbine, the wind speed in front of the blade increases. Affected by wind shear and the tower, the wind speed curve is not in a completely symmetrical state. The wind speed at the summit is affected by wind acceleration and wake, which further increases the wind speed near the summit. As the height increases, the wind speed gradually returns to the state before the influence of wind turbines. The position behind the mountain is far from the wind turbine. Except for the backflow area which is affected by the wake of the wind turbine, the curves at other positions remain basically consistent with those before the wind turbine's influence.

Fig. 10a shows the velocity cloud diagram of the central symmetry plane of the wind turbine when it is shut down. As the wind turbine stops rotating, the overall wind speed, apart from being affected by the blades and the tower, does not fluctuate much, and the wind profile remains basically the same as before the wind turbine was installed. Fig. 10b–d respectively show the speed curves of the three position points in front of the mountain, at the top of the mountain, and behind the mountain when the wind turbine is shut down and there is no wind turbine. It can be clearly seen in Fig. 10a that the wind speed curve is lower than that when there is no wind turbine. This is because when the wind turbine is not rotating, the only factor

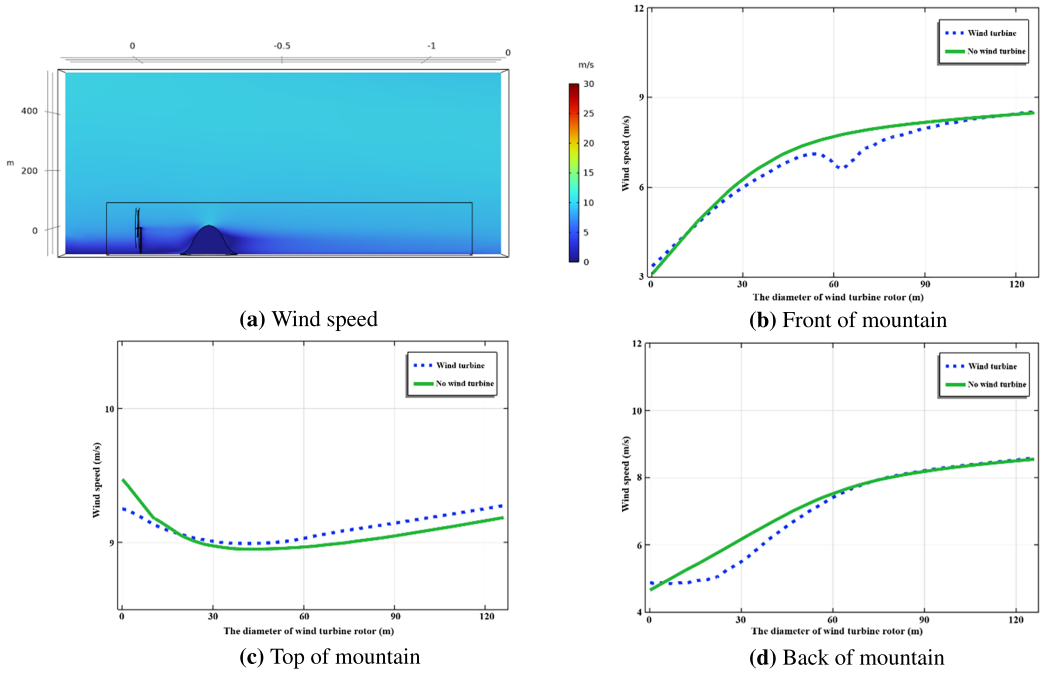
affecting the wind speed is the wind turbine itself. Because the wind turbine was placed 2 days in front of the center of the mountain, the wind speed here was most affected. The wind speed at the center of the wind wheel decreased further due to the influence of the hub. Fig. 10b,c are relatively far from the wind turbine, and the impact can be ignored.



(a) Wind speed **(b)** Front of mountain

(c) Top of mountain **(d)** Back of mountain

Figure 9: Speed cloud map and wind speed profile of the wind turbine rotates.



(a) Wind speed **(b)** Front of mountain

(c) Top of mountain **(d)** Back of mountain

Figure 10: Wind speed cloud maps and wind speed profiles with and without wind turbines when wind turbine stops.

The above-mentioned wind speed and power were normalized. Taking the center of the wind turbine as the origin and the radius of the wind turbine as the reference, five wind measurement points were selected from top to bottom, namely −1, −0.5, 0, 0.5 and 1. The specific positions are shown in Fig. 11. The wind speed and power were normalized with the power corresponding to the wind speed of 8 m/s as the expected value. The sorted data are shown in Table 1.

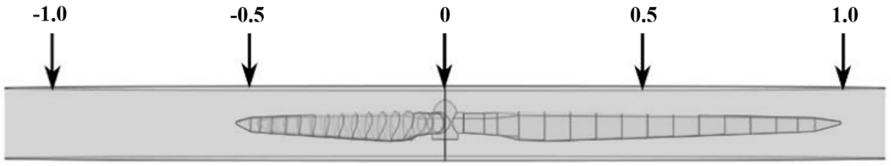


Figure 11: Distance from the center of wind turbine.

Table 1: Wind speed and power corresponding to the wind turbine at different positions in front of the mountain after normalization.

Position and Status of the Wind Turbine	Distance from the Center of Wind Turbine					Average Speed	Power
	−1	−0.5	0	0.5	1		
Rotate (front)	0.5475	1.1163	1.1000	0.8088	0.7388	0.8623	0.6669
Stop (front)	0.4200	0.7688	0.8350	1.0138	1.0650	0.8205	0.5583
Rotate (top)	1.2325	1.1638	1.0325	1.1513	1.1588	1.1478	1.5511
Stop (top)	1.1563	1.1250	1.1300	1.1450	1.1600	1.1433	1.5336
Rotate (back)	0.9188	1.1225	0.8825	1.0838	1.0750	1.0165	1.0610
Stop (back)	0.6100	0.7050	0.9513	1.0363	1.0738	0.8753	0.7007

The average wind speed and power data of the wind turbine were extracted and plotted as bar charts and line graphs, as shown in Fig. 12. When the wind turbine was in the upstream position, the wind speed in front of the mountain was between 0.8 and 0.9 of the expected wind speed. When the wind turbine was rotating, it reached 0.67 of the expected power, and when it was not rotating, it was 0.56. The wind speed and power at the summit position both exceeded expectations. The wind speed was approximately 1.14, and the power was 1.5. The position behind the mountain can only reach the expected wind speed and power when the wind turbine is rotating. When it is not rotating, the wind speed is 0.87 of the expected value and the power is 0.7 of the expected value.

(2) The wind turbine is located on the top of the mountain

As shown in Fig. 13, it is the calculation domain and cross-sectional diagram of the wind turbine at the top of the mountain. The grid encryption area is further enhanced, and the near-ground area and the wind turbine jointly perform grid encryption.

Fig. 14a shows the velocity cloud map of the central symmetry plane of the wind turbine in operation. The wake trajectory of the wind turbine can be clearly seen in the figure. Due to the rotation of the wind turbine, the superposition with the wind acceleration effect generates a large-scale reflux area, causing the downward movement of the terrain wake to mix with the flow that forms a reflux upward movement in the terrain wake. The wake is initially gradually developed downward under the induction of the terrain. However, due to the excessive slope of the terrain, the wake trajectory cannot move downward along the leeward side. The lower boundary of the wake reaches its lowest point at the foot of the mountain. After

passing through the foot of the mountain, the induction of the terrain disappears, and the center of the wake gradually returns to the center of the wind wheel. Fig. 14b–d respectively show the speed curves of the wind turbine in operation at the three measurement points in front of the mountain, at the top of the mountain, and behind the mountain with or without the wind turbine. It can be seen from Fig. 13b that the air flow velocity in front of the mountain is not affected by other factors. Fig. 14c shows that after acceleration through the wind peak, the overall flow velocity has increased to a certain extent, reaching 10.76 m/s. Fig. 14d shows the outline of the wind behind the mountain. Due to the mixture of the reflux area and the wake area of the wind turbine, the wind speed behind the mountain is generally higher than that in the state without wind turbines, with the maximum wind speed reaching 11.20 m/s.

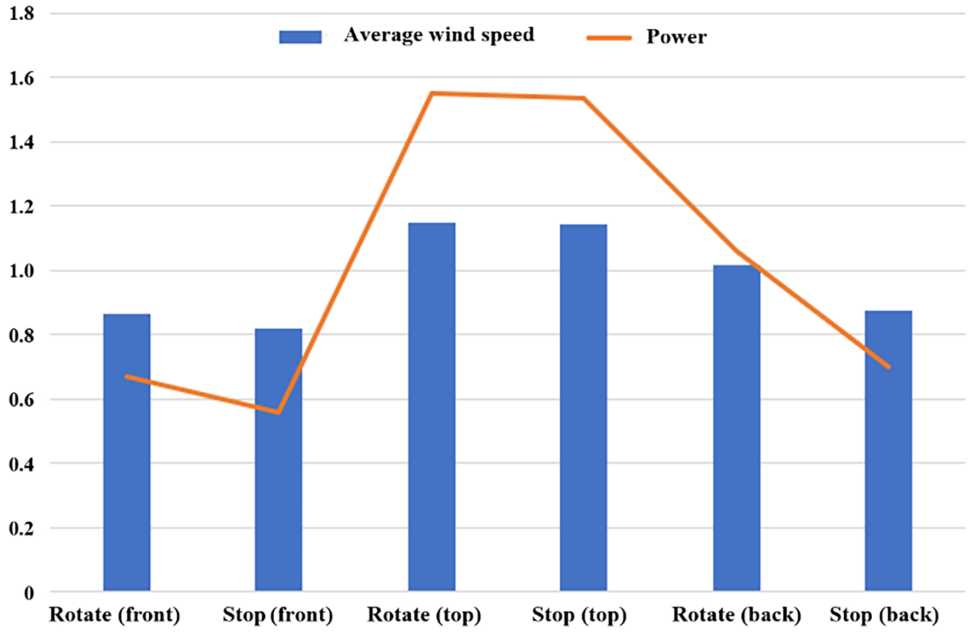
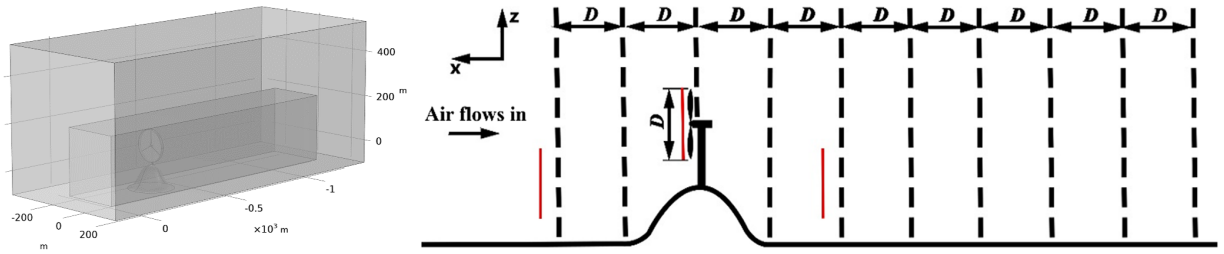


Figure 12: Average wind speed and power corresponding to the stationary state of wind turbine at different positions.



(a) Fluid calculation domain **(b)** Analytical cross-section

Figure 13: Fluid calculation domain and analysis cross-section.

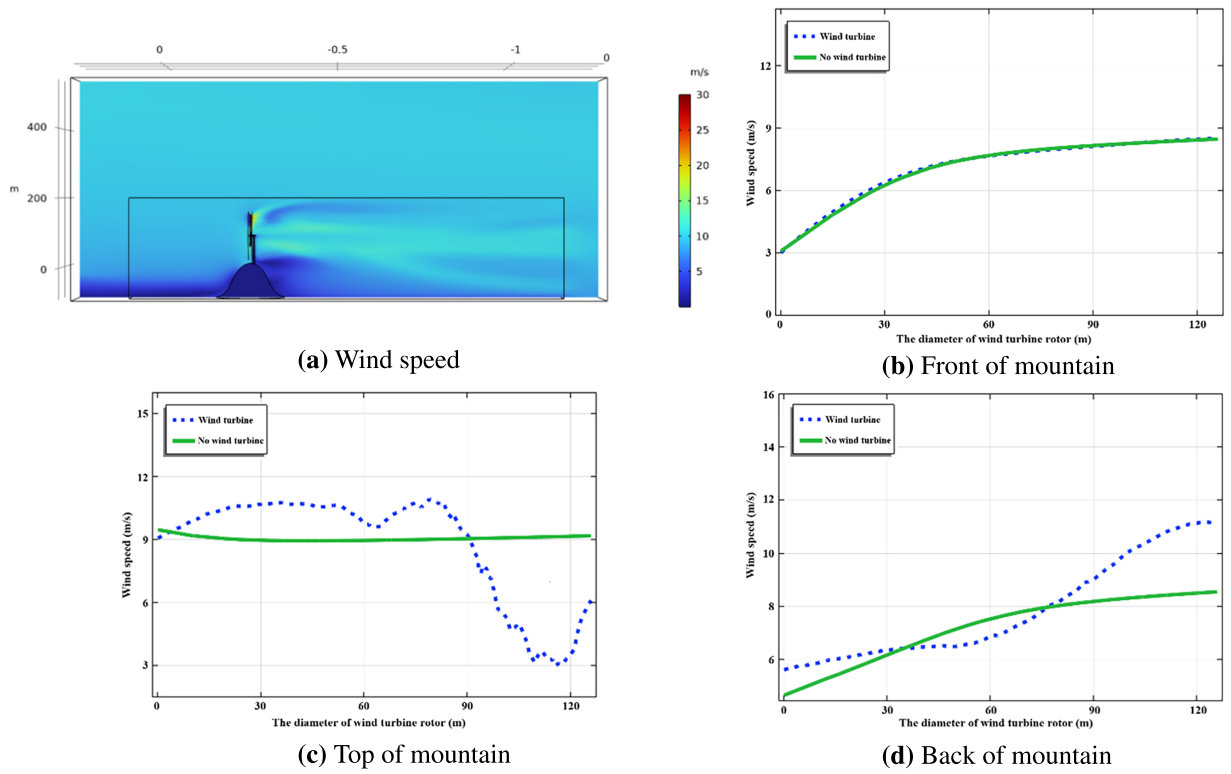


Figure 14: The wind speed cloud map and wind speed profile with or without wind turbine rotates.

Fig. 15a shows the velocity cloud diagram of the central symmetry plane when the wind turbine is at the top of the mountain and has stopped rotating. The wind speed in front of the mountain is the same as that when there is no wind turbine due to the absence of obstructions. At the top of the mountain, the wind is blocked by the wind turbine, causing the wind speed at the summit to decrease. As the height increases, the wind speed returns to its initial state. The area behind the mountain is jointly influenced by the mountain and the wind turbines, which affects the wind speed acceleration effect. The leeward slope reflux area is divided into two parts: one part is the reflux area generated by the mountain itself, and the other part is the reflux area generated between the bottom of the wind turbine tower and the mountain. The superposition of the two reduces the overall wind speed in the area behind the mountain. Moreover, the wind speed will further decrease at the horizontal line where the mountain meets the wind turbine. Fig. 15b–d respectively show the speed curves of the wind turbine when it is at the top of the mountain and in the shutdown state with or without the wind turbine. Fig. 15b shows the wind speed at the front of the mountain. Without the influence of other factors, the calculation result of the wind speed remains unchanged. Fig. 15c shows that the wind acceleration effect is weakened due to the influence of the wind turbine tower. When the air flows through the center of the wind turbine, the speed gradually returns to the initial state. Fig. 15d shows that due to the combined effect of the mountain and the wind turbine, the overall wind speed is in a decreasing state. The minimum wind speed occurs on the horizontal line where the wind turbine contacts the mountain, which is 4.32 m/s.

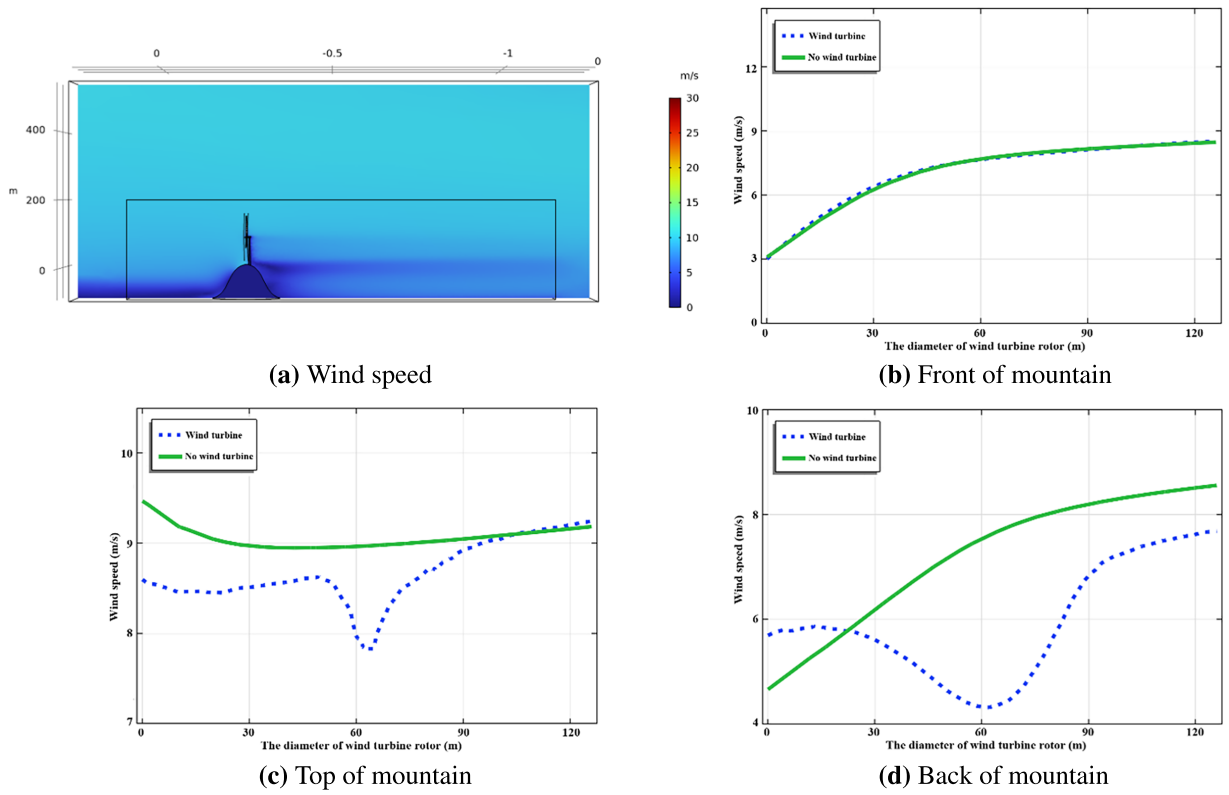


Figure 15: The wind speed cloud map and wind speed profile with or without wind turbine stops.

Table 2 shows the wind speeds corresponding to different positions under different states of the wind turbine, as well as the corresponding average wind speeds and power after data normalization. As shown in Fig. 16, when the wind turbine is at the top of the mountain, the calculated wind speed value remains basically consistent as mentioned above. The wind speed and power at the summit position can both reach the expected values. The position behind the mountain is close to the expected wind speed and power when the wind turbine is in operation. When not in operation, the wind speed is 0.76 of the expected value and the power is 0.4 of the expected value.

Table 2: Wind speed and power corresponding to different positions at the top of the mountain after normalization.

Position and Status of the Wind Turbine	Distance from the Center of Wind Turbine					Average Speed	Power
	−1	−0.5	0	0.5	1		
Rotate (front)	0.3775	0.8112	0.9763	1.0250	1.0663	0.8513	0.6383
Stop (front)	0.3763	0.8338	0.9775	1.0250	1.0650	0.8555	0.6493
Rotate (top)	1.1338	1.3375	1.2688	0.9463	0.7625	1.0898	1.3321
Stop (top)	1.075	1.065	0.9888	1.1263	1.1563	1.0823	1.3043
Rotate (back)	0.7025	0.8013	0.9138	1.1738	1.3875	0.9958	0.9898
Stop (back)	0.7125	0.6825	0.5600	0.8963	0.9613	0.7625	0.4073

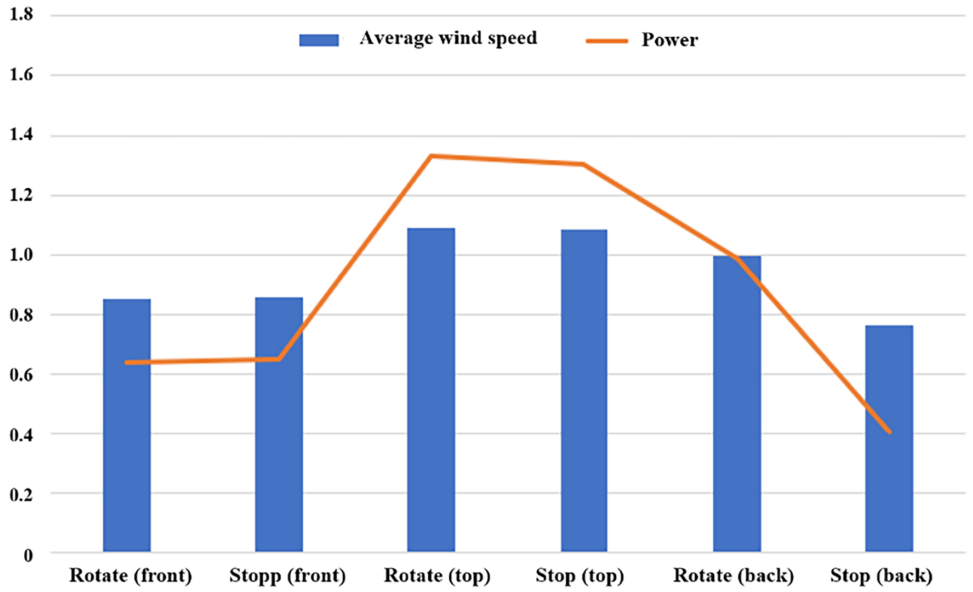
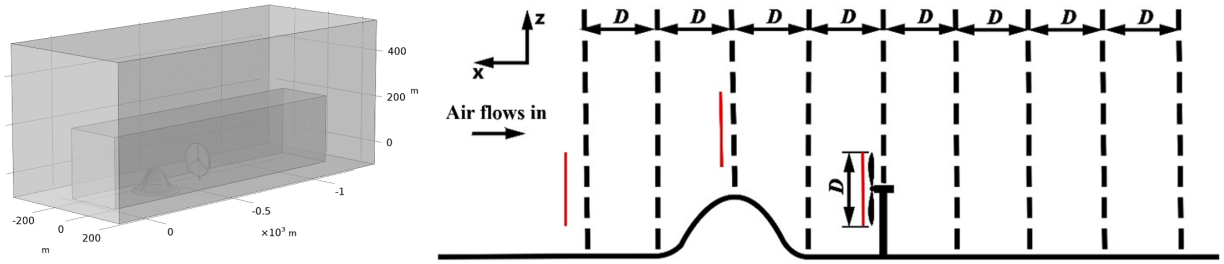


Figure 16: The average wind speed and power corresponding to different positions and states of wind turbines.

(3) The wind turbine is located downstream of the terrain

As shown in Fig. 17, it is the calculation basin and cross-sectional diagram of the wind turbine located 2D downstream from the center of the mountain. The wind speed measurement area is the diameter D of the wind turbine (the part in the red area).



(a) Fluid calculation domain **(b)** Analytical cross-section

Figure 17: Fluid calculation domain and analysis cross-section.

Fig. 18a shows the velocity cloud map of the wind turbine located on the central symmetry plane downstream of the mountain when it is in operation. The wake trajectory of the wind turbine can be clearly observed in the figure. At the beginning, the wake center is at the center of the wind turbine, and then it slightly floats upward. The reason for this is that the wind turbine is placed outside the backflow area. The wind speed here is accelerated by the mountaintop wind and flows closely to the backflow area from top to bottom, making the wind speed here generally higher than that at the front of the mountain. Therefore, the wind turbine wake has a tendency to float upward and will return to the initial state as the distance increases. Fig. 18b–d respectively show the wind speed curves when the wind turbine is operating at the three positions of the front of the mountain, the top of the mountain, and the back of the mountain with or without the wind turbine. As Fig. 18b,c are not affected, the wind speed calculation results are consistent with the aforementioned calculation results. Fig. 18d shows that due to the acceleration of the mountaintop wind, the

wind speed at the lower part of the wind wheel increases, while the wind speed at the upper part gradually returns to the initial state as the height increases.

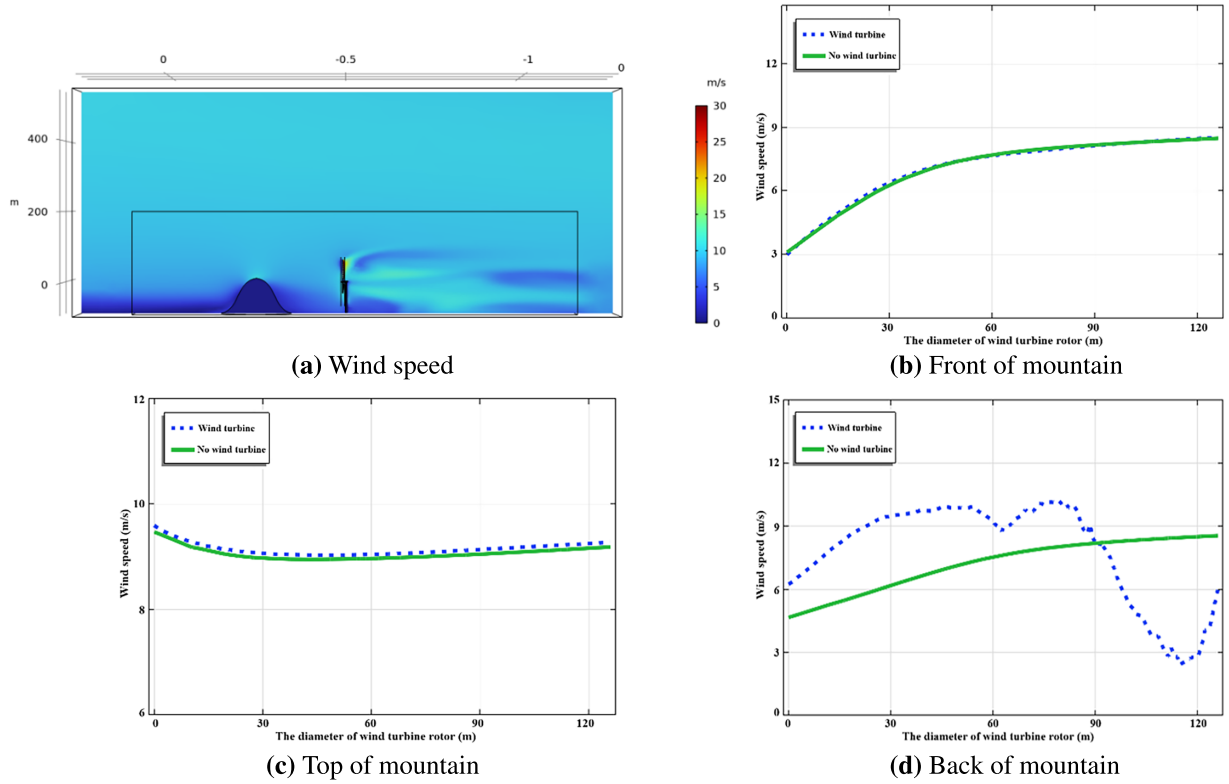
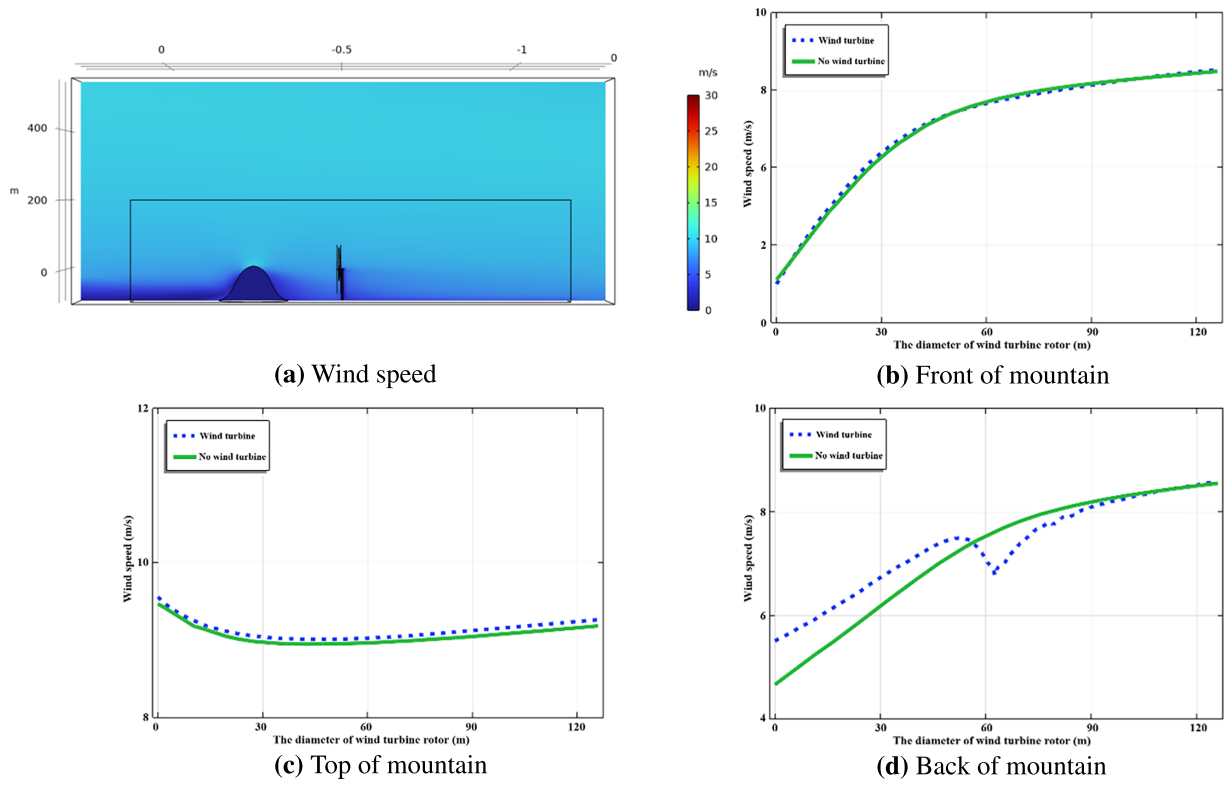


Figure 18: The wind speed cloud map and wind speed profile with or without wind turbine rotates.

Fig. 19a shows the velocity cloud map of the wind turbine located on the central symmetry plane downstream of the mountain when it is shut down. It can be clearly seen that the impact brought by the wind turbine when it is shut down is very small and basically consistent with the calculated wind speed value when there is no wind turbine. Fig. 19b–d respectively show the wind speed curves at the three position points of the front, top, and back of the mountain when the wind turbine is at the back of the mountain and in the shutdown state. It can be seen that the curves in Fig. 19b,c are consistent with those during the operation of the wind turbine and are not affected by other factors. Fig. 19d shows that the wind speed is relatively low below the center of the wind turbine due to the influence of the tower.

Table 3 shows the wind speeds corresponding to different positions of the wind turbine under different states after data normalization, as well as the corresponding average wind speeds and power.

As shown in Fig. 20, when the wind turbine is in the downstream position, the wind speed in front of the mountain is 0.85 of the expected wind speed, and when the wind turbine is in operation, it reaches 0.64 of the expected power. The wind speed and power at the summit position both exceeded expectations. The wind speed was approximately 1.15, and the power was 1.6. The position behind the mountain did not meet expectations. When the wind turbine was rotating, the wind speed reached the expected 0.96 and the power was 0.91. When it stopped rotating, the wind speed was 0.9 and the power was 0.78.



(a) Wind speed

(b) Front of mountain

(c) Top of mountain

(d) Back of mountain

Figure 19: The wind speed cloud map and wind speed profile with or without wind turbine stops.

Table 3: Wind speed and power corresponding to different positions at the back of mountain after normalization.

Position and Status of the Wind Turbine	Distance from the Center of Wind Turbine					Average Speed	Power
	−1	−0.5	0	0.5	1		
Rotate (front)	0.3738	0.8201	0.9675	1.0251	1.0663	0.8505	0.6363
Stop (front)	0.3738	0.8203	0.9850	1.0251	1.0663	0.8540	0.6454
Rotate (top)	1.2001	1.1313	1.1325	1.145	1.1588	1.1535	1.5736
Stop (top)	1.1953	1.1288	1.1313	1.144	1.1588	1.1515	1.5658
Rotate (back)	0.7801	1.1938	1.2238	0.8763	0.7475	0.9642	0.9142
Stop (back)	0.6875	0.8525	0.9825	1.0251	1.0754	0.9065	0.7756

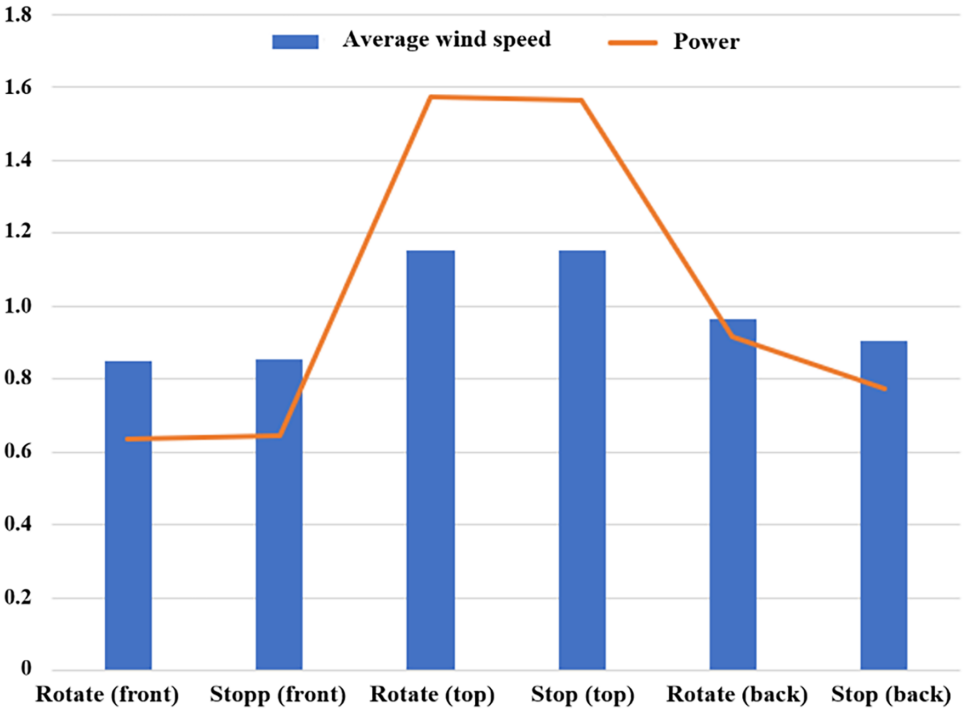


Figure 20: Average wind speed and power corresponding to different positions and states of wind turbines.

5 Data Discussion

For the study of the influence of terrain roughness, the geographical location and state of wind turbines on the flow velocity and power of wind farms in complex terrains, it can be analyzed that:

(1) By importing the simplified model and selecting four different terrain roughness, the wind shear function with a wind speed of 8 m/s at a height of 90 m above the ground was chosen as the entry wind speed. In front of the mountain, since it is only affected by the terrain roughness, the wind speed contour lines all show an exponential function distribution. The wind speed differences from the maximum to the minimum surface roughness are 7.86, 8.33, 8.43 and 8.501 m/s, respectively. It can be seen from this that as the surface roughness decreases, the wind speed is less affected by the wind shear effect. At the summit, due to the influence of the mountain, there will be a distinct wind acceleration effect near the ground at the summit. The smaller the roughness, the more obvious the acceleration effect. The measurement position selected at the back of the mountain was not in the reflux zone, so the wind speed was not affected by the reflux zone. The wind speed near the ground at the top of the mountain would closely follow the reflux zone and flow towards lower areas, resulting in an overall higher wind speed at the back of the mountain. As the height changed, the wind speed returned to the magnitude of the wind shear velocity.

(2) After importing the wind turbine model, place the wind turbines in front of, at the top of and behind the mountain, respectively, and normalize the obtained wind speed data against the power. When the wind turbine is at the front of the mountain, the average wind speeds before going down the mountain when the wind turbine is rotating and stationary are 0.8623 and 0.8205, respectively, and the corresponding powers are 0.6669 and 0.5583. At the summit, the corresponding wind speeds are 1.1478 and 1.1433, and the powers are 1.5511 and 1.5336. The corresponding wind speeds behind the mountain are 1.0165 and 0.8753, and the corresponding powers are 1.0610 and 0.7007. When the wind turbine

is at the top of the mountain, the average wind speeds before going down the mountain when it is rotating and stationary are 0.8513 and 0.8555, respectively, and the corresponding powers are 0.6383 and 0.6493. At the top of the mountain, the corresponding wind speeds are 1.0898 and 1.0823, and the powers are 1.3321 and 1.3043. The corresponding wind speeds behind the mountain are 0.9958 and 0.7625, and the corresponding powers are 0.9898 and 0.4073. When the wind turbine is at the back of the mountain, the average wind speeds before going down the mountain when it is rotating and stationary are 0.8505 and 0.8540, respectively, and the corresponding powers are 0.6363 and 0.6454. At the summit, the corresponding wind speeds are 1.1535 and 1.1515, and the powers are 1.5736 and 1.5658. The corresponding wind speeds behind the mountain are 0.9642 and 0.9065, and the corresponding powers are 0.9142 and 0.7756.

(3) By placing a wind turbine at the front and the top of the mountain, respectively, the ground roughness was increased to simulate the wind speed changes under special circumstances. The roughness increased from small to large. The average wind speeds at the front of the mountain were 0.8318 and 0.8208, and the corresponding powers were 0.5876 and 0.5590. The average wind speeds at the summit position are 1.0735 and 1.0863, corresponding to powers of 1.2720 and 1.3191. The average wind speeds at the back of the mountain are 0.7368 and 0.6688, corresponding to power levels of 0.3693 and 0.2632.

6 Conclusion

Under the condition that the terrain roughness changes, the speed difference within the measurement range of the mountain front position increases as the roughness decreases. At the summit position near the ground, the wind speed is significantly increased due to the wind acceleration effect. However, as the height increases, the influence of wind acceleration begins to decrease. The main component of the speed gradually becomes the wind speed corresponding to the wind shear function. The smaller the terrain roughness, the more obvious the acceleration effect. The wind speed is the lowest in the flow area formed behind the mountain. The larger the terrain roughness, the larger the flow area. However, the measurement position is far from the flow area and is not affected by it. The overall wind speed here increases and gradually returns to the size of the wind shear wind speed as the height increases.

Combine the wind turbine with the three-dimensional mountain area to analyze and measure the wind speed and power in the measurement area. When the wind turbine is located in front of the mountain, whether it rotates or not, it cannot reach the expected power. The power of the wind turbine corresponding to this position is below 0.7 of the expected power. The wind speed at the summit can exceed the expected power after wind acceleration. The power at the back of the mountain can reach 1.5 times the expected power under the condition that the wind turbine is rotating. When the wind turbine is located at the top of the mountain, the power at the front of the mountain fails to meet the expected requirements. The wind speed at the summit is higher than expected, and the power can reach 1.3 times the expected power. The wind speed and power at the back of the mountain can only barely meet expectations when the wind turbine is rotating. When the wind turbine is located at the back of the mountain, the wind power at the top of the mountain reaches 1.57 times the expected level. Behind the mountain, the wind turbine can barely reach the expected power when rotating, and only 0.7 of the expected power when it stops rotating under special circumstances. Under the conditions of two wind turbines and changes in ground roughness, the power at the position in front of the mountain is only below the expected 0.6. The position of the mountain top can still meet the expected requirements. The position behind the mountain is affected by multiple wind turbines. When the roughness is normal, the expected power reaches 0.37, but when the roughness is too large, the power is only the expected 0.26.

Acknowledgement: Not applicable.

Funding Statement: The authors received no specific funding for this study.

Author Contributions: Xin Guan conceived the study, designed the methodology, and conducted the experiments. Bo Liu performed data analysis and visualization with support from Hao Tang. Dechen Kong contributed the theoretical framework and supervised the computational modeling. Longlong Zong drafted the manuscript, with critical revisions provided by all co-authors. All authors reviewed and approved the final version of the manuscript.

Availability of Data and Materials: The Askervein Hill measurement data used to support the findings of this study are publicly available. The simulation data generated during the current study are available from the corresponding author on reasonable request.

Ethics Approval: Not applicable. This study does not involve human participants or animal experiments.

Conflicts of Interest: The authors declare no conflicts of interest.

References

1. Michos D, Catthoor F, Foussekis D, Kazantzidis A. Ultra-short-term wind power forecasting in complex terrain: a physics-based approach. Energies. 2024;17(21):5493. doi:10.3390/en17215493.
2. Wang X, Hu J, Deng K, Zhang M, Shen S, Shen Y, et al. Study on wind farm flow field characteristics based on boundary condition optimization of complex mountain numerical simulation. Processes. 2024;12(9):1885. doi:10.3390/pr12091885.
3. Duque EPN, Burklund MD, Johnson W. Navier-stokes and comprehensive analysis performance predictions of the NREL phase VI experiment. J Sol Energy Eng. 2003;125(4):457–67. doi:10.1115/1.1624088.
4. Kondo K, Tsuchiya M, Sanada S. Evaluation of effect of micro-topography on design wind velocity. J Wind Eng Ind Aerodyn. 2002;90(12–15):1707–18. doi:10.1016/S0167-6105(02)00281-7.
5. Cao S, Tamura T. Effects of roughness blocks on atmospheric boundary layer flow over a two-dimensional low hill with/without sudden roughness change. J Wind Eng Ind Aerodyn. 2007;95(8):679–95. doi:10.1016/j.jweia.2007.01.002.
6. Ishihara T, Fujino Y, Hibi K. A wind tunnel study of separated flow over a two dimensional ridge and a circular hill. J Wind Eng Ind Aerodyn. 2001;89:573–6. doi:10.1016/s0167-6105(99)00064-1.
7. Tian W, Ozbay A, Yuan W, Sarakar P, Hu H, Yuan W. An experimental study on the performances of wind turbines over complex terrain. In: Proceedings of the 51st AIAA Aerospace Sciences Meeting Including the New Horizons Forum and Aerospace Exposition; 2013 Jan 7–10; Grapevine, TX, USA. p. 1–14. doi:10.2514/6.2013-612.
8. Hyvärinen A, Segalini A. Effects from complex terrain on wind-turbine performance. J Energy Resour Technol. 2017;139(5):051205. doi:10.1115/1.4036048.
9. Shapiro CR, Gayme DF, Meneveau C. Filtered actuator disks: theory and application to wind turbine models in large eddy simulation. Wind Energy. 2019;22(10):1414–20. doi:10.1002/we.2376.
10. Karim A, Adrien T, Dominique A, Frédéric MY. Towards prediction of wind load on pylons for a neutral atmospheric boundary layer flow over two successive hills. J Wind Eng Ind Aerodyn. 2021;208:104402. doi:10.1016/j.jweia.2020.104402.
11. Tian W, Ozbay A, Hu H. An experimental investigation on the aeromechanics and wake interferences of wind turbines sited over complex terrain. J Wind Eng Ind Aerodyn. 2018;172(1):379–94. doi:10.1016/j.jweia.2017.11.018.
12. Yan B, Tang S, Yu M, Qian G, Chen Y. Atmospheric turbulence effects on wind turbine wakes over two-dimensional hill: a wind tunnel study. Energies. 2025;18(11):2865. doi:10.3390/en18112865.
13. Chen X, Ishihara T. Numerical study of turbulent flows over complex terrain using an unsteady Reynolds-averaged Navier-Stokes model with a new method for turbulent inflow generation. J Wind Eng Ind Aerodyn. 2025;257(2):105991. doi:10.1016/j.jweia.2024.105991.

14. Yamaguchi A, Tavana A, Ishihara T. Assessment of wind over complex terrain considering the effects of topography, atmospheric stability and turbine wakes. Atmosphere. 2024;15(6):723. doi:10.3390/atmos15060723.
15. Li L, Yang Q, Pan H. Multiscale flow simulation of complex terrain wind farm under unsteady wind. Acta Energiae Solaris Sin. 2022;43(11):179–85. (In Chinese).
16. Lee JH, Kim S, Ryu JH. Optimal wind farm layout in a complex terrain by varying turbine hub heights: case study of yeongdeok, South Korea. Energies. 2026;19(4):1109. doi:10.3390/en19041109.
17. Li S, Ge W, Cheng Y, Zhang J. Quantitative study of a generic model of complexity taking into account topographic features. Hydrogr Surv Charting. 2024;2:72–7. (In Chinese).
18. Wu Z, Lv B, Chen B, Wang G, Wan Y, Zhao B, et al. Vertical wind speed extrapolation and power estimation via a hybrid physics-data-driven approach. Energies. 2026;19(5):1302. doi:10.3390/en19051302.
19. Cheng Y. Research on fine numerical simulation and modeling of tail flow in wind turbine units under complex atmospheric conditions. Beijing, China: University of Chinese Academy of Sciences; 2020. (In Chinese).